ELMO and Sponge specify subapical restriction of Canoe and formation of the subapical domain in early Drosophila embryos

Anja Schmidt*, Zhiyi Lv*, Jörg Großhans

* equal contribution

Institute for Developmental Biochemistry
University of Göttingen,
Justus-von-Liebig Weg 11
37077 Göttingen
Germany

corresponding authour
Jörg Großhans, email: joerg.grosshans@med.uni-goettingen.de

Key words

Drosophila, cortical domains, epithelial domains, epithelial polarity, subapical, F-actin, small GTPase, guanyl nucleotide exchange factor, cellularisation, cellularization,

Summary statement

The unconventional guanyl nucleotide exchange factor complex ELMO-Sponge restricts the actin binding protein Canoe/Afadin to the subapical region during cellularization in Drosophila embryos.

Abstract

Canoe/Afadin and the GTPase Rap1 specify the subapical domain during cellularization in Drosophila embryos. The timing of domain formation is unclear. The subapical domain may gradually mature or emerge synchronously with basal and lateral domain. The mechanism for activation of Rap1 by potential guanyl nucleotide exchange factors (GEF) or GTPase activating proteins (GAP) is unknown. Here, we retraced the emergence of the subapical domain at the onset of cellularization by in vivo imaging with CanoeYFP in comparison to the lateral and basal markers, ScribbledGFP and CherrySlam. CanoeYFP accumulates at a subapical position at about the same time as the lateral marker ScribbledGFP but a few minutes prior to basal CherrySlam. Furthermore, we show that the unconventional GEF complex ELMO-Sponge is subapically enriched and is required for subapical restriction of Canoe. The localization dynamics of ELMO-Sponge suggests a patterning mechanism for positioning the subapical region adjacent to the apical region. While marking the disc-like apical regions before cellularization, ELMO-Sponge redistributes to a ring-like pattern surrounding the apical region at the onset of cellularization.

Introduction

Cortical domains, i. e. apical, subapical, lateral, basal domains, are a characteristic feature of epithelial cells and are crucial for their diverse functions (Hermiston and Gordon, 1995; Martín-Belmonte et al., 2008; Stephenson et al., 2010). Cortical domains are defined by integral membrane proteins, such as Crumbs and E-Cadherin as well as membrane associated proteins such as Par proteins (Chalmers et al., 2005; Cohen et al., 2004; Izumi et al., 1998) in addition to lipid composition (reviewed in Gassama-Diagne and Payrastre 2009). In many cases the separation of the domains

is maintained by mutual exclusion of determinants, like lateral exclusion of Bazooka (Baz)/Par-3 by Par-1 and Scribbled (Scrib) (Benton and Johnston, 2003, Bilder et al., 2003). In contrast, the mechanisms for initial establishment and arrangement of cortical regions are less clear.

During embryonic development of Drosophila, epithelial cells emerge in the cellular blastoderm stage in a process called cellularization. Following a stage of syncytial development including 13 nuclear cycles, about 6000 cortical nuclei are synchronously enclosed into individual cells in interphase 14, in that the plasma membrane invaginates between adjacent nuclei (reviewed in Foe et al., 1993). Cellularization leads to a monolayered columnar epithelium with four distinct cortical regions and adherens junctions positioned at the subapical region. Prior to cellularization, only two cortical regions can be differentiated, cap and intercap regions in the syncytial embryos (Warn et al., 1980; Warn et al., 1984). During mitosis of the nuclear cycles, the spindles are separated by an up to 10 µm deep metaphase furrow (Sherlekar and Rikhy, 2017). Three cortical regions are found within the metaphase furrow, apical, lateral, and the basal region (Mavrakis et al., 2009). The change of cellular organization and switch from syncytial to cellular development is a central feature of the mid blastula transition (MBT) beside cell cycle remodeling, degradation of maternal RNA and activation of zygotic transcription (reviewed in Farrell and O'Farrell, 2014; Liu and Großhans, 2017; Yuan et al., 2016).

Here we focus on the subapical region, which in contrast to the other cortical regions, emerges during cellularization. It has been suggested that the subapical region gradually matures, since Baz/Par-3, the typical subapical determinant, and the E-Cadherin complex gradually accumulate during the course of cellularization and are properly positioned only by the end of cellularization (Harris and Peifer, 2004; McGill et al., 2009). Subapical restriction of Baz and E-Cadherin depends on the actin binding protein Canoe/Afadin (Cno) and its regulator, the Rap1 GTPase (Choi et al., 2013, Sawyer et al., 2009). Histological analysis of fixed embryos suggested that Canoe marks the subapical domain prior to Baz (Choi et al., 2013). The timing of initial subapical accumulation of Canoe has not been retraced. Being a GTPase, Rap1 is potentially regulated by an upstream guanyl nucleotide exchange factor (GEF) or a GTPase activating factor (GAP). The unconventional GEF complex ELMO/Ced-12-Sponge/DOCK (Spg) may represent a candidate (Geisbrecht et al., 2008; Postner et

al., 1992, Winkler et al., 2015). Biochemical analysis indicates that ELMO-DOCK complexes are GEF specific for Rac and Rap1 (Biersmith et al., 2011; Biersmith et al., 2015; deBakker et al., 2004; Yajnik et al. 2003; Wu and Horvitz, 1998). Although a function of *sponge* for organization of actin caps in syncytial embryos has been reported some time ago (Postner et al., 1992), a function in context of the subapical domain or Canoe has not been investigated, yet.

In this study, we show by live imaging that cortical markers Canoe, Scribbled and Slam segregate during the first minutes of cellularization. Analyzing the mutant phenotypes of *ELMO* and *sponge*, we identify them as an upstream factor of Canoe localization. We report the dynamics of Sponge and ELMO protein in fixed and live embryos. Sponge and ELMO mark the apical regions, which are characterized by strong F-actin staining (“actin caps”) of the plasma membrane during the syncytial blastoderm stage prior to cellularization. Strikingly, this localization pattern changes at the onset of cellularization. ELMO and Sponge redistribute to the rims of the actin caps and surround the apical regions and thus generates the information for a new region. Essentially, the pattern changes from a disc-like to a ring-like pattern. Based on this dynamic, we propose a model for pattern formation in that the subapical domain is positioned adjacent to the apical domain.

Results

Emergence of the subapical domain during onset of cellularization

Stereotypic and stage specific changes in cortical organization are linked to early embryonic development (Nance et al., 2014). In Drosophila, a uniformly structured cortex is characteristic for the preblastoderm stage (Karr and Alberts, 1986). When the first nuclei reach the cortex in nuclear cycle 9, their associated centrosomes induce cortical differentiation and segregation of cortical markers into disc-like caps or cytoplasmic buds, rich in F-actin and the region between the caps (intercap), which is marked by Slam and Toll (Fig. 1A, Mavrakis et al., 2009; Raff and Glover, 1989; Warn et al., 1984). The cortex is further differentiated during syncytial mitoses. By immunostaining, we detected three cortical domains: Slam at the furrow tip, Discs-large (Dlg) at the furrow and Canoe apically and at the furrow (Fig. 1B).

An important feature of MBT and the transition from syncytial to cellular development is the emergence of a subapical domain and of a typical epithelial cortex with four domains. The subapical domain is inserted between the apical and lateral domain. Canoe is the most-upstream acting subapical marker (Choi et al., 2013). During syncytial mitoses. We detected Canoe at the apical and lateral regions. Staining was excluded from the basal domain (Fig. 1C). The cortical distribution profoundly changes in interphase 14, when we detected Canoe restricted to the subapical domain and segregated from the lateral marker Dlg (Fig 1D, E). In contrast to Canoe, other subapical markers such as Baz, Par-6, aPKC and E-Cadherin accumulate gradually at the subapical region during the course of cellularization (Harris and Peifer, 2004; McGill et al., 2009; Wang et al., 2004).

To achieve a precise timing and reveal the dynamics of subapical accumulation of Canoe, we conducted time lapse imaging of embryos expressing CanoeYFP from its endogenous locus in comparison with the lateral marker ScribbledGFP or the basal marker CherrySlam (Fig. 2, Supplemental data Fig. 1, 2). As we reported previously (Acharya et al., 2014), Slam continuously marks the transition from the retracting metaphase furrows to cellularization furrows (“old” furrow). Within a delay of a few minutes, Slam accumulated at the “new” furrow. For comparative timing, we referred to the formation of the furrow between corresponding daughter nuclei and retraction of the metaphase furrow. During telophase, the retracting metaphase furrow (“old” furrow) encloses corresponding daughter nuclei, while a shallow groove (“new” furrow) emerges between them (Fig. 2A).

We found that CanoeYFP (Fig. 2 A, B, t=3 min) and ScribbledGFP (Fig. 2 A, C, t=1 min) were uniformly dispersed following retraction of the metaphase furrow. Within a few minutes, however, a restriction of both markers became visible at the prospective furrow (Fig. 2B, C, t=7 min). CherrySlam accumulated slightly later than CanoeYFP at the new furrow. A clear signal was observed starting at t=8 to 12 min (Fig. 2B, D, E). This difference between CanoeYFP and CherrySlam was also observed along the apical-basal axis. CanoeYFP reached its high levels at a position between 2–3 µm (Fig. 2D, E). CherrySlam showed the strongest signal a few minutes later at a position of about 4 µm (Fig. 2D, E). The appearance of CherrySlam in the basal layer is probably linked to the invagination of the new furrow. These data describe a clear

segregation of the subapical and basal marker already at t=8 min. This represents the first time that the two markers were clearly separated.

We could also detect a difference for accumulation of the lateral marker, ScribbledGFP. We detected a strong signal at position 3–5 µm (Fig. 2F), which was more basal than the peak of CanoeYFP. Domain restriction and furrow formation also become obvious by considering the width of the new furrow (Fig. 2G, Supplemental data Fig. S3). Within 10 min, the width of the CanoeYFP region was gradually reduced from 2.5 µm to 0.5 µm. In summary, our live imaging analysis shows that the cortical domains form within about 10 min after exit from mitosis 13. Both analysis of fixed and live embryos show that Canoe marks the subapical domain throughout cellularization and thus suggests that the subapical domain forms together with the basal and lateral domains and does not gradually arise during cellularization.

Staining and live analysis revealed a mutually exclusive distribution of Canoe, Scribbled and Slam. We asked whether this pattern depended on the function of these proteins. We first confirmed previous reports that membrane association of Canoe depended on Rap1 (Choi et al., 2013, Fig. 3A, B). In contrast, subapical Canoe restriction did neither depend on *slam* (Fig. 3E) nor *scribbled* (Fig. 3D). We stained embryos from *scribbled* or *slam* germline clones, in the following named *scribbled* and *slam* mutant embryos, for Canoe and the lateral marker Dlg. In *scribbled* mutants, we detected subapically restricted Canoe (Fig. 3D). Consistent with previous reports about the mutual dependency of Scribbled and Dlg (Bilder et al., 2003), Dlg was spread over and loosely associated with the membrane in *scribbled* mutants. Similarly, Canoe was subapically restricted in *slam* mutants (Fig. 3E). Although furrow invagination is impaired, furrows are specified in *slam* mutants (Acharya et al., 2014). These data show that the initial accumulation of the subapical marker Canoe does not depend on *scrib* and *slam* and that the independent pathways on the level of *canoe*, *scribbled* and *slam* may define the respective cortical domains.

The unconventional GEF complex ELMO – Sponge controls subapical Canoe restriction

The GTPase Rap1 is presumably controlled by GEF or GAP proteins, such as the GEF protein Dizzy (Dzy) (Huelsmann et al., 2006; Spahn et al., 2012) or the heteromeric GEF complex, ELMO – Sponge (Fig. 4E; Biersmith et al., 2011; Yajnik et al., 2003). To test this hypothesis, we analyzed *dizzy* mutant embryos for subapical restriction of

Canoe. In embryos from *dizzy* germline clones, we did not detect a deviation of Canoe staining as compared to wild type embryos (Fig. 3C). In contrast, Canoe was spread along the cellularization furrow in embryos from *ELMO* germline clones (Fig. 5B, D,) and embryos from *sponge* females (Fig. 5C). These embryos are in the following designated as *ELMO* and *sponge* embryos. *ELMO* embryos passed through a normal number of nuclear divisions, but failed to form actin caps and metaphase furrows during syncytial cycles (Fig. 4B; Winkler et al., 2015). Associated with this morphological phenotype were chromosomal segregation defects and subsequent nuclear fall-out. In interphase 14, they cellularized at the anterior and posterior termini but not in the medial region (Fig. 4C). We observed a similar phenotype in *sponge* embryos, which is consistent with a previous report (Postner et al., 1992).

Canoe spread along the cellularization furrows in *ELMO* and *sponge* embryos, whereas the lateral marker Dlg and the basal marker Slam normally localized (Fig. 5B, C). We quantified the distribution of Canoe along the cellularization furrow by plotting the relative fluorescence along the apical-basal axis. We did not compare absolute protein levels. Whereas restriction to the subapical domain was observed in wild type embryos (Fig. 5A, D), Canoe was spread all along the furrow in *ELMO* embryos (Fig. 5B, D). These data show that *ELMO* and *sponge* are required for subapical restriction of Canoe.

Subapical restriction of ELMO and Sponge during cellularization

Functioning upstream of Canoe, the ELMO-Sponge complex may confer positional information for the subapical domain, in that ELMO or Sponge would localize to the prospective subapical region latest when subapical restriction of Canoe is observed. To test this hypothesis, we analyzed the dynamics and localization pattern of ELMO and Sponge. Since a suitable antibody was available (Biersmith et al., 2011), we fixed and stained wild type embryos for Sponge (Fig. 6). We detected Sponge at the caps in syncytial cycles. During syncytial mitoses, uniform Sponge staining was detected at the apical and lateral membranes. A strikingly different pattern was observed in embryos during cellularization. We detected a staining pattern clearly restricted to the subapical domain and largely separated from the lateral marker Dlg throughout cellularization (interphase 14). The subapical restriction of Sponge was not as clear as what we observed for Canoe, however. Importantly, Sponge staining was depleted in

the apical region, leading to a grid-like pattern in the surface view even when the apical most layers were included in the projections (Fig. 6).

The subapical staining pattern of Sponge depended neither on *scribbled, canoe* nor *Rap1*. We detected subapical restriction of Sponge in *scribbled*, *Rap1 and canoe* germline clones, in the following named *scribbled*, *Rap1* and *canoe* mutants (Fig. 7A–D). These data indicate that Sponge functions independently and possibly upstream of the Rap1-Canoe pathway. In contrast to *Rap1, canoe* and *scribbled*, subapical localization of Sponge depends on *ELMO*. We stained *ELMO* mutants for Sponge. Sponge signal was uniformly distributed and no membrane association was detected (Fig. 7E). The loss of membrane association and restricted localization is consistent with the structure of the ELMO-Sponge complex, in which ELMO provides membrane binding and Sponge the GEF activity (Fig. 4E, Komander et al., 2008).

To record the dynamics of the ELMO-Sponge complex in high temporal resolution, we generated an ELMO-GFP fusion protein expressed from a genomic transgene (Fig. 4A). The ELMO-GFP fusion protein was expressed in comparable levels as the wild type allele (Fig. 4D) and is functional, as it rescues the germline clone phenotype of *ELMO*. During syncytial cycles, we detected ELMO-GFP at the caps (Fig. 8A). With the onset of cellularization the localization pattern of ELMO-GFP profoundly changed. The ELMO-GFP signal changed from the disc-like pattern in syncytial interphases to a ring-like pattern (Fig. 8B, C, arrowheads; Supplemental data Fig. S4). ELMO-GFP signal at new furrows were first detected at about the time, when CanoeYFP accumulated at the apical region (Fig. 2). We quantified the relative fluorescence intensity along the apical-basal axis of new furrows and compared the profile to CherrySlam fluorescence (Fig. 8D). In summary, we observed an early subapical accumulation and subsequent restriction of ELMO-GFP, whereas CherrySlam accumulated a few minutes later at a basal position.

Discussion

In this study, we have focused on analysis of functional relationships of cortical domains and their associated proteins to insert a new domain at a specific time and place. Based on in vivo and in vitro studies of ELMO-Sponge/DOCK, Rap1 and Canoe/Afadin in other experimental systems, we have some understanding of their biochemical activities (Biersmith et al., 2011; Boettner et al., 2003; Sawyer et al., 2009). In biochemical assays, the ELMO-Sponge complex specifically activates Rac and Rap1 among the small GTPases (Yajnik et al., 2003). ELMO-Sponge may activate the Rap1 in the subapical region during the onset of cellularization (Fig. 9). As a consequence, activated Rap1-GTP may restrict Canoe to the subapical domain. We analyzed the distribution of Rap1 employing Rap1-GFP as a proxy. As we detected a wide and uniform distribution of Rap1-GFP over the plasma membrane (Supplemental data Fig. S4), Rap1 distribution cannot be used as a test for whether ELMO-Sponge would activate Rap1. Alternatively, ELMO-Sponge may act on Canoe independently of Rap1 (Fig. 9), as we have not demonstrated that Rap1 links ELMO-Sponge and Canoe or that Rap1 is activated by ELMO-Sponge.

During the course of cellularization, Canoe will gradually recruit the polarity protein Bazooka/Par-3 and subsequently the E-Cadherin complex to this domain to make it to a generic subapical domain. When comparing the distribution of ELMO-Sponge and Canoe, Canoe is more clearly localized than ELMO-Sponge. This difference may be due to the signaling process. In the simple model, the pathway initiated by ELMO-Sponge via Rap1 and Canoe is linear. We do not rule out reinforcing feed-back interactions within the pathway that can lead to enhanced signals. Such feed-back interactions are likely to be important for maintenance of the subapical domain. For example, Baz influences Canoe localization later in cellularization (Choi et al., 2013). In the accompanying paper, Bonello et al., (2017) describe a function of *dizzy* for the apical restriction and especially localization of Canoe to tricellular junctions via activation of Rap1 during late cellularization.

When studying the initial formation of the subapical domain, we have not observed an influence of the lateral determinant Scribbled or the basal protein Slam. Such interactions are likely to be important later in cellularization and development for maintenance of the cortical domains or sharpening of the boundaries, as it is well

established that lateral and subapical components interact by mutually exclusion (Bilder et al., 2003; Tanentzapf and Tepass, 2003).

The change in ELMO-Sponge distribution from a disc-like pattern during the nuclear cycles to a ring-like pattern during initial cellularization suggests a model for the origin of positional information for the emerging subapical domain (Fig. 9A). The organization in cap and intercap regions already contains the information for a third domain, namely the interface between the two regions (Fig. 9B). The dynamical localization pattern of ELMO-Sponge makes use of this information in initial cellularization. Whereas being uniformly distributed within the caps during syncytial cycles, ELMO-Sponge accumulates at the rimes of the apical region during onset of cellularization. Subsequently, when the furrows invaginate, adjacent rings around the apical regions meet to form a grid-like pattern.

The determinants for specific membrane localization of ELMO-Sponge are not clear. Within the ELMO-Sponge complex (Fig. 4E), membrane association is assumed to be conferred by ELMO. The role of the conserved ELMO domain is unclear (Komander et al., 2008). The PH domain may mediate membrane association by binding phospholipids. However, no corresponding subapical localization pattern of phospholipids has been reported, so far. Sensor proteins for $PI(4,5)P_2$ and $PI(3,4,5)P_3$ were reported to be widely distributed along the invaginating furrow (Reversi et al., 2014). As an alternative to phospholipids, a membrane protein may serve as an anchor for ELMO.

The change of ELMO-Sponge distribution from a disc- to ring-like pattern coincides with the mid blastula transition. Thus, the change from disc- to ring-like pattern may ultimately depend on one or more zygotic genes, on cell cycle regulators, such as checkpoint kinases, which change their activity during MBT or other MBT associated processes (reviewed in Liu and Großhans, 2017). Among the early zygotic genes, the best candidate contributing to ELMO-Sponge redistribution may be the zygotic gene *dunk*, which controls apical myosin contractility and flow at the onset of cellularization. However, a potential role of *dunk* or other zygotic genes for cortical domain formation and segregation has not been analyzed (He et al., 2016). Future experiments analyzing the detailed dynamics and factors controlling localization of ELMO-Sponge may provide insight into the underlying molecular and biophysical mechanism.

Material and Methods

Fly strains and genetics

Fly stocks were obtained from the Bloomington stock center, if not otherwise noted. Following fly strains and mutations were used: UASp-CherrySlam, driven by maternal Gal4 (Acharya et al., 2014), Df(2L)*slam* (Acharya et al., 2014), ced-12/*ELMO*^{367} (Winkler et al., 2015), *cno*[R2] (Choi et al., 2013), CanoeYFP (*PBac{602.P.SVS-1}cno*^{CPTI000590}, Kyoto stock center), *scrb-GFP*^{CA07683} (Buszczak et al., 2007), *scrb[1]* (Bilder and Perrimon, 2000), *rap1*[P5709] (R. Reuter, Knox and Brown, 2002), *sponge*[242] (Postner et al., 1992), Df(3R)3450 (deficiency uncovering *sponge*), *dizzy(Δ8)* (R. Reuter, Huelsmann et al., 2006), GFP-Rap1 (Elisabeth Knust; Knox and Brown, 2002). ELMO-GFP transgenes were generated according to standard protocols by PhiC31 integrase-mediated site-specific insertions in the landing site ZH-86Fb (Bischof et al., 2007). All fly cages and crosses were maintained by standard methods at 25°C unless otherwise specified. Germline clones were induced by heat shock (each 1 h, at 24–48 h and 48–72 h of development) of first and second instar larvae and selected by ovoD transgenes on corresponding Frt chromosomes.

Molecular genetics

The genomic ELMO-GFP construct was generated by ligation of multiple fragments, which were amplified by PCR. Fragment 1-GFP (optimized for Drosophila codon usage), upstream primer ZL95 (tggcggccgc ACTGGAAGTT CTGTTCCAGG GGCCCGGCTC CGCCGGCTCC), introducing a NotI site and a PreScission cleavage site, and downstream primer ZL75 (TAAAGCTTGT ACAGCTCGTC CATGCC), inserting a HindIII site. Fragment 2-ELMO3' with a leading stop codon (chromosome 2L, 12,100543–12,101,303), upstream primer ZL76 (ACAAGCTTTA AGCATAACGA GCACAATTAC), adding a stop codon and HindIII site, and downstream primer ZL73 (atctcgaGTC TGCCTGCCGG ACCGG), adding a XhoI site to the 3' site. Both fragments were cloned into pBSK (NotI/Xho1) leading to BSK-GFP-ELMO3' and transferred to the transformation vector pAttB (pAttB-GFP-ELMO3'). Fragment 3: genomic DNA from the *ELMO* locus with a size of 3633 bp including 5' region of ELMO locus until the 3' end of ELMO exon 4 (chromosome 2L, 12,096,904–12,100,537). NotI

sites were introduced on both ends by upstream primer ZL99 (AACAGATCTG CGGCCGGAAG ACAAGCGATC GGATGC) and downstream primer ZL104 (ACTTCCAGTg cggccgcgCT CTCAAAGCAA AAATCATAG). Fragment 3 was cloned into the NotI site of pAttB-GFP-ELMO3' leading to the final transformation plasmid pAttB-ELMO-GFP-ELMO3', comprising DNA from the *ELMO* locus region (breakpoints are 12,096,904–12,101,303) with a PreScission cleavage site and GFP in front of the stop codon.

Immunostaining

Embryos were fixed by 4% formaldehyde or heat fixed according to standard procedures described before (Großhans et al., 2005) and stored in methanol. Fixed embryos were rinsed thrice in in phosphate buffered saline (PBS) with 0.1% Tween20 (PBT), and blocked in 5% bovine serum albumin (BSA) in PBT for 1 h at room temperature. Blocked embryos were incubated with primary antibodies in 0.1% BSA in PBT overnight at 4°C or at room temperature for 2 h with constant rotation. After rinsing thrice and washing four times for 15 min with PBT, the embryos were incubated with fluorescently labelled secondary antibodies in PBT for 2 h at room temperature. Following another round of rinsing and washing, embryos were stained with DAPI (0.2 µg/ml) for 10 min, rinsed thrice in PBT, washed in PBT for 10 min and mounted in Aquapolymount (Polysciences). Embryos for phalloidin staining were fixed by 8% formaldehyde and vitelline membrane was manually removed. Following antibodies were used: Primary antibodies: rabbit-anti-Canoe (1:1000, Choi et al., 2013), mouse-anti-Dlg (1:100, 4F3, Hybridoma Center), rabbit-/guinea pig-anti-Slam (1:5000, Brandt et al., 2006), guinea pig-anti-Sponge (1:1000, Biersmith et al., 2011); Phalloidin coupled to Alexa 488 (Thermo Fisher). Secondary antibodies Alexa Fluor 488, 568, and 647 antibodies (1:500, Thermo Fisher).

Western blots

Western blots were conducted as previously described (Wenzl et al., 2010). Briefly, lysis samples of staged embryos (0–2 h) corresponding to 10 embryos were separated by SDS polyacrylamide electrophoresis and transferred by wet transfer to a nitrocellulose membrane. Blots were imaged with an Odyssey CLx Infrared imaging system with 16 bit depth. Primary antibodies: goat-anti-ELMO (1:3000, Biersmith et al., 2011), mouse-anti-α-Tubulin (1:50000, B512, Sigma). Secondary antibodies (800CW,

680CW, Donkey anti-guinea pig/mouse/rabbit IgG). Images were processed by Adobe Photoshop and FIJI/ImageJ (Schindelin et al., 2015).

Imaging

Living embryos were handled as described before (Kanesaki et al., 2011). Fluorescent time lapse movies and images of fixed embryos were recorded with a confocal microscope (Zeiss LSM780, equipped with Airyscan detection, objectives LCI Plan Neofluar 63×/water NA 1.3 for fixed samples, Plan Neofluar 63×/oil NA 1.4 for live imaging). Movies of embryos expressing CanoeYFP and CherrySlam were obtained with a frame size of 256x256 pixel (28.7x28.7 µm) and a lateral pixel size of 110 nm in an interval of 60 s. Channels were changed after recording of every z-Stack. Z-stacks had 19 slices with a step size of 0.5 µm. Embryos expressing ScribbledGFP were imaged with Airyscan detection with a frame size of 488x488 pixel (36x36 µm) and a lateral pixel size of 73 nm. Every z-stack included 11 slices with a step size of 1 µm, that was imaged in an interval of 60 s. Embryos expressing ELMO-GFP and CherrySlam were imaged with Airyscan detection with a frame size of 488x488 pixel (32x32 µm) with a lateral pixel size of 66 nm. Every z-stack contained 17 slices with a step size of 0.5 µm, that was obtained in an interval of 60s. Images of embryos expressing GFP-Rap1 were obtained with Airyscan detection with a frame size of 476x476 pixel (32.1x32.1 µm; 67,5 nm lateral pixel size). Z-stacks were conducted with a step size of 0.2 µm and orthogonal views were conducted with Fiji/ImageJ as well as measuring of furrow length. Fixed embryos were imaged with a frame size of 512x512 pixel (67.5x67.5 µm; 130 nm lateral pixel size) for top views and 512x200 pixel (96.4x29.4 µm; 190 nm lateral pixel size) for sagittal views. Images were processed with Fiji/ImageJ and Adobe Photoshop and Adobe Illustrator..

Image quantification

Measurements were conducted with Fiji/ImageJ, calculation with Microsoft Excel. For quantifications in Fig. 2E, F and 8D fluorescence intensities were measured along three furrows in each z position along the apical-basal axis. The maximal intensities for each protein were normalized to 1 and plotted as a graph with apical-basal position on the y axis and normalized fluorescence intensities on the x axis. The heatmap in Fig. 5D was prepared by measuring the fluorescence intensity distribution along the

furrows in side views in total 9 furrows in 3 embryos. Intensities were normalized to 1 for every furrow and displayed as heatmaps using the conditional formatting function in Microsoft Excel. Averages of normalized intensities were plotted with apical-basal position on the y axis and normalized fluorescence intensities on the x axis. For quantifications in Fig. 2G, the distribution of CanoeYFP fluorescence intensity at one furrow was measured in top view of live images at different time points using the line plot function of Fiji/ImageJ. Position zero on the x axis was defined by the peak of the curve at the latest time point. For the graph in Fig. 2H, the width of the CanoeYFP signal at three furrows was measured at different time points in top view of live images and plotted against the time.

Acknowledgements

We are grateful to E Geisbrecht, D Bilder, M Peifer, R Reuter, E. Knust for materials or discussions. We acknowledge service support from the Developmental Studies Hybridoma Bank created by NICHD of the NIH/USA and maintained by the University of Iowa, the Bloomington Drosophila Stock Center (supported by NIH P40OD018537), the Drosophila Genomics and Genetic Resources, Kyoto, the BACPAC Resources Center at Children's Hospital Oakland and the Genomic Resource Center at Indiana University (supported by NIH 2P40OD010949-10A1). ZL was in part supported by a fellowship from the China Scholarship Council. This work was in part supported by the Göttingen Centre for Molecular Biology (funds for equipment repair) and the Deutsche Forschungsgemeinschaft (Priority programme SPP1464, GR1945/4-1/2, and equipment grant INST1525/16-1 FUGG).

Competing interests

No competing interests declared.

References

Acharya, S., Laupsien, P., Wenzl, C., Yan, S., Großhans, J., (2014). Function and dynamics of slam in furrow formation in early Drosophila embryo. *Dev. Biol.* **386**, 371–384. doi:10.1016/j.ydbio.2013.12.022

Benton, R., Johnston, D.S. (2003). Drosophila PAR-1 and 14-3-3 Inhibit Bazooka/PAR-3 to Establish Complementary Cortical Domains in Polarized Cells. *Cell* **115**, 691–704. doi:10.1016/S0092-8674(03)00938-3

Biersmith, B., Liu, Z., Bauman, K., Geisbrecht, E.R. (2011). The DOCK Protein Sponge Binds to ELMO and Functions in Drosophila Embryonic CNS Development. *PLOS ONE* **6**, e16120. doi:10.1371/journal.pone.0016120

Biersmith, B., Wang, Z.-H., Geisbrecht, E.R. (2015). Fine-Tuning of the Actin Cytoskeleton and Cell Adhesion During Drosophila Development by the Unconventional Guanine Nucleotide Exchange Factors Myoblast City and Sponge. *Genetics* **200**, 551–567. doi:10.1534/genetics.115.177063

Bilder, D., Perrimon, N. (2000). Localization of apical epithelial determinants by the basolateral PDZ protein Scribble. *Nature* **403**, 676–680. doi:10.1038/35001108

Bilder, D., Schober, M., Perrimon, N. (2003). Integrated activity of PDZ protein complexes regulates epithelial polarity. *Nat. Cell Biol*. **5**, 53–58. doi:10.1038/ncb897

Bischof, J., Maeda, R.K., Hediger, M., Karch, F., Basler, K. (2007). An optimized transgenesis system for Drosophila using germ-line-specific phiC31 integrases. *Proc. Natl. Acad. Sci. U.S.A*. **104**, 3312–3317. doi:10.1073/pnas.0611511104

Boettner, B., Harjes, P., Ishimaru, S., Heke, M., Fan, H.Q., Qin, Y., Aelst, L.V., Gaul, U. (2003). The AF-6 Homolog Canoe Acts as a Rap1 Effector During Dorsal Closure of the Drosophila Embryo. *Genetics* **165**, 159–169.

Bonello, T. T., Perez-Vale, K. Z., Sumigray, K. D., Peifer, M. (2017). Rap1 acts via multiple mechanisms to position Canoe/Afadin and adherens junction and thus mediate apical-basal polarity establishment Development in revision/accompanying manuscript

Brandt, A., Papagiannouli, F., Wagner, N., Wilsch-Bräuninger, M., Braun, M., Furlong, E.E., Loserth, S., Wenzl, C., Pilot, F., Vogt, N., Lecuit, T., Krohne, G., Großhans, J. (2006). Developmental Control of Nuclear Size and Shape by kugelkern and kurzkern. *Current Biology* **16**, 543–552. doi:10.1016/j.cub.2006.01.051

Buszczak, M., Paterno, S., Lighthouse, D., Bachman, J., Planck, J., Owen, S., Skora, A.D., Nystul, T.G., Ohlstein, B., Allen, A., Wilhelm, J.E., Murphy, T.D., Levis, R.W., Matunis, E., Srivali, N., Hoskins, R.A., Spradling, A.C. (2007). The Carnegie Protein Trap Library: A Versatile Tool for Drosophila Developmental Studies. *Genetics* **175**, 1505–1531. doi:10.1534/genetics.106.065961

Chalmers, A.D., Pambos, M., Mason, J., Lang, S., Wylie, C., Papalopulu, N. (2005). aPKC, Crumbs3 and Lgl2 control apicobasal polarity in early vertebrate development. *Development* **132**, 977–986. doi:10.1242/dev.01645

Choi, W., Harris, N.J., Sumigray, K.D., Peifer, M. (2013). Rap1 and Canoe/afadin are essential for establishment of apical-basal polarity in the Drosophila embryo. *Mol. Biol. Cell* **24**, 945–963. doi:10.1091/mbc.E12-10-0736

Cohen, D., Brennwald, P.J., Rodriguez-Boulan, E., Müsch, A. (2004). Mammalian PAR-1 determines epithelial lumen polarity by organizing the microtubule cytoskeleton. *J Cell Biol* **164**, 717–727. doi:10.1083/jcb.200308104

deBakker, C.D., Haney, L.B., Kinchen, J.M., Grimsley, C., Lu, M., Klingele, D., Hsu, P.-K., Chou, B.-K., Cheng, L.-C., Blangy, A., Sondek, J., Hengartner, M.O., Wu, Y.-C., Ravichandran, K.S. (2004). Phagocytosis of apoptotic cells is regulated by a UNC-73/TRIO-MIG-2/RhoG signaling module and armadillo repeats of CED-12/ELMO. *Curr. Biol.* **14**, 2208–2216. doi:10.1016/j.cub.2004.12.029

Farrell, J.A., O'Farrell, P.H. (2014). From egg to gastrula: How the cell cycle is remodeled during the Drosophila mid-blastula transition. *Annu Rev Genet* **48**, 269–294. doi:10.1146/annurev-genet-111212-133531

Foe, V.E., Odell, G.M., Edgar, B.A. (1993). *Mitosis and morphogenesis in the Drosophila embryo: Point and counterpoint,* in: The Development of Drosophila Melanogaster, M. Bate and A. Martinez Arias. pp. 149–300. Cold Spring Harbor Laboratory,

Gassama-Diagne, A., Payrastre, B. (2009). Phosphoinositide signaling pathways: promising role as builders of epithelial cell polarity. *Int Rev Cell Mol Biol* **273**, 313–343. doi:10.1016/S1937-6448(08)01808-X

Geisbrecht, E.R., Haralalka, S., Swanson, S.K., Florens, L., Washburn, M.P., Abmayr, S.M. (2008). Drosophila ELMO/CED-12 interacts with Myoblast city to direct myoblast fusion and ommatidial organization. *Dev Biol* **314**, 137–149. doi:10.1016/j.ydbio.2007.11.022

Großhans, J., Wenzl, C., Herz, H.-M., Bartoszewski, S., Schnorrer, F., Vogt, N., Schwarz, H., Müller, H.-A. (2005). RhoGEF2 and the formin Dia control the formation of the furrow canal by directed actin assembly during Drosophila cellularisation. *Development* **132**, 1009–1020. doi:10.1242/dev.01669

Harris, T.J.C., Peifer, M. (2004). Adherens junction-dependent and -independent steps in the establishment of epithelial cell polarity in Drosophila. *J Cell Biol* **167**, 135–147. doi:10.1083/jcb.200406024

He, B., Martin, A., Wieschaus, E. (2016). Flow-dependent myosin recruitment during Drosophila cellularization requires zygotic dunk activity. *Development* **143**, 2417–2430. doi:10.1242/dev.131334

Hermiston, M.L., Gordon, J.I. (1995). In vivo analysis of cadherin function in the mouse intestinal epithelium: essential roles in adhesion, maintenance of differentiation, and regulation of programmed cell death. *J Cell Biol* **129**, 489–506. doi:10.1083/jcb.129.2.489

Huelsmann, S., Hepper, C., Marchese, D., Knöll, C., Reuter, R. (2006). The PDZ-GEF Dizzy regulates cell shape of migrating macrophages via Rap1 and integrins in the Drosophila embryo. *Development* **133**, 2915–2924. doi:10.1242/dev.02449

Izumi, Y., Hirose, T., Tamai, Y., Hirai, S., Nagashima, Y., Fujimoto, T., Tabuse, Y., Kemphues, K.J., Ohno, S. (1998). An Atypical PKC Directly Associates and Colocalizes at the Epithelial Tight Junction with ASIP, a Mammalian Homologue of Caenorhabditis elegans Polarity Protein PAR-3. *J Cell Biol* **143**, 95–106.

Kanesaki, T., Edwards, C.M., Schwarz, U.S., Grosshans, J. (2011). Dynamic ordering of nuclei in syncytial embryos: a quantitative analysis of the role of cytoskeletal networks. *Integr Biol (Camb)* **3**, 1112–1119. doi:10.1039/c1ib00059d

Karr, T.L., Alberts, B.M. (1986). Organization of the cytoskeleton in early Drosophila embryos. *J Cell Biol* **102**, 1494–1509. doi:10.1083/jcb.102.4.1494

Knox, A.L., Brown, N.H. (2002). Rap1 GTPase Regulation of Adherens Junction Positioning and Cell Adhesion. *Science* **295**, 1285–1288. doi:10.1126/science.1067549

Komander, D., Patel, M., Laurin, M., Fradet, N., Pelletier, A., Barford, D., Côté, J.-F. (2008). An alpha-helical extension of the ELMO1 pleckstrin homology domain mediates direct interaction to DOCK180 and is critical in Rac signaling. *Mol. Biol. Cell* **19**, 4837–4851. doi:10.1091/mbc.E08-04-0345

Liu, B., Grosshans, J. (2017). Link of Zygotic Genome Activation and Cell Cycle Control, in: Zygotic Genome Activation, Methods in Molecular Biology. pp. 11–30. Humana Press, New York, NY, doi:10.1007/978-1-4939-6988-3_2

Martín-Belmonte, F., Yu, W., Rodríguez-Fraticelli, A.E., Ewald, A., Werb, Z., Alonso, M.A., Mostov, K. (2008). Cell Polarity Dynamics Controls the Mechanism of Lumen Formation in Epithelial Morphogenesis. *Curr Biol* **18**, 507–513. doi:10.1016/j.cub.2008.02.076

Mavrakis, M., Rikhy, R., Lippincott-Schwartz, J. (2009). Plasma membrane polarity and compartmentalization are established before cellularization in the fly embryo. *Dev Cell* **16**, 93–104. doi:10.1016/j.devcel.2008.11.003

McGill, M.A., McKinley, R.F.A., Harris, T.J.C. (2009). Independent cadherin-catenin and Bazooka clusters interact to assemble adherens junctions. *J Cell Biol* **185**, 787–796. doi:10.1083/jcb.200812146

Nance J (2014). Getting to know your neighbor: cell polarization in early embryos. *J Cell Biol.* **206**, 823–832. doi: 10.1083/jcb.201407064.

Postner, M.A., Miller, K.G., Wieschaus, E.F. (1992). Maternal effect mutations of the sponge locus affect actin cytoskeletal rearrangements in Drosophila melanogaster embryos. *J Cell Biol* **119**, 1205–1218.

Raff, J.W., Glover, D.M. (1989). Centrosomes, and not nuclei, initiate pole cell formation in Drosophila embryos. *Cell* **57**, 611–619. doi:10.1016/0092-8674(89)90130-X

Reversi, A., Loeser, E., Subramanian, D., Schultz, C., De Renzis, S. (2014). Plasma membrane phosphoinositide balance regulates cell shape during Drosophila embryo morphogenesis. *J Cell Biol* **205**, 395–408. doi:10.1083/jcb.201309079

Sawyer, J.K., Harris, N.J., Slep, K.C., Gaul, U., Peifer, M. (2009). The Drosophila afadin homologue Canoe regulates linkage of the actin cytoskeleton to adherens junctions during apical constriction. *J Cell Biol* **186**, 57–73. doi:10.1083/jcb.200904001

Schindelin, J., Rueden, C.T., Hiner, M.C., Eliceiri, K.W. (2015). The ImageJ ecosystem: An open platform for biomedical image analysis. *Mol. Reprod. Dev*. **82**, 518–529. doi:10.1002/mrd.22489

Sherlekar, A., Rikhy, R. (2017). Syndapin bridges the membrane-cytoskeleton divide during furrow extension. *Commun Integr Biol* **10**. doi:10.1080/19420889.2016.1255832

Spahn, P., Ott, A., Reuter, R. (2012). The PDZ-GEF protein Dizzy regulates the establishment of adherens junctions required for ventral furrow formation in Drosophila. *J Cell Sci* **125**, 3801–3812. doi:10.1242/jcs.101196

Stephenson, R.O., Yamanaka, Y., Rossant, J. (2010). Disorganized epithelial polarity and excess trophectoderm cell fate in preimplantation embryos lacking E-cadherin. *Development* **137**, 3383–3391. doi:10.1242/dev.050195

Tanentzapf, G., Tepass, U. (2003). Interactions between the crumbs, lethal giant larvae and bazooka pathways in epithelial polarization. *Nat Cell Biol* **5**, 46–52. doi:10.1038/ncb896

Wang, F., Dumstrei, K., Haag, T., Hartenstein, V. (2004). The role of DE-cadherin during cellularization, germ layer formation and early neurogenesis in the Drosophila embryo. *Dev Biol* **270**, 350–363. doi:10.1016/j.ydbio.2004.03.002

Warn, R.M., Bullard, B., Magrath, R. (1980). Changes in the distribution of cortical myosin during the cellularization of the Drosophila embryo. *Development* **57**, 167–176.

Warn, R.M., Magrath, R., Webb, S. (1984). Distribution of F-actin during cleavage of the Drosophila syncytial blastoderm. *J Cell Biol*. **98**, 156–162.

Wenzl, C., Yan, S., Laupsien, P., Großhans, J. (2010). Localization of RhoGEF2 during Drosophila cellularization is developmentally controlled by Slam. *Mech. Dev.* **127**, 371–384. doi:10.1016/j.mod.2010.01.001

Winkler, F., Gummalla, M., Künneke, L., Lv, Z., Zippelius, A., Aspelmeier, T., Großhans, J. (2015). Fluctuation Analysis of Centrosomes Reveals a Cortical Function of Kinesin-1. *Biophys J* **109**, 856–868. doi:10.1016/j.bpj.2015.07.044

Wu, Y.C., Horvitz, H.R. (1998). C. elegans phagocytosis and cell-migration protein CED-5 is similar to human DOCK180. *Nature* **392**, 501–504. doi:10.1038/33163

Yajnik, V., Paulding, C., Sordella, R., McClatchey, A.I., Saito, M., Wahrer, D.C.R., Reynolds, P., Bell, D.W., Lake, R., van den Heuvel, S., Settleman, J., Haber, D.A. (2003). DOCK4, a GTPase activator, is disrupted during tumorigenesis. *Cell* **112**, 673–684.

Yuan, K., Seller, C.A., Shermoen, A.W., O'Farrell, P.H. (2016). Timing the Drosophila Mid-Blastula Transition: A Cell Cycle-Centered View. *Trends Genet* **32**. doi:10.1016/j.tig.2016.05.006

Figures

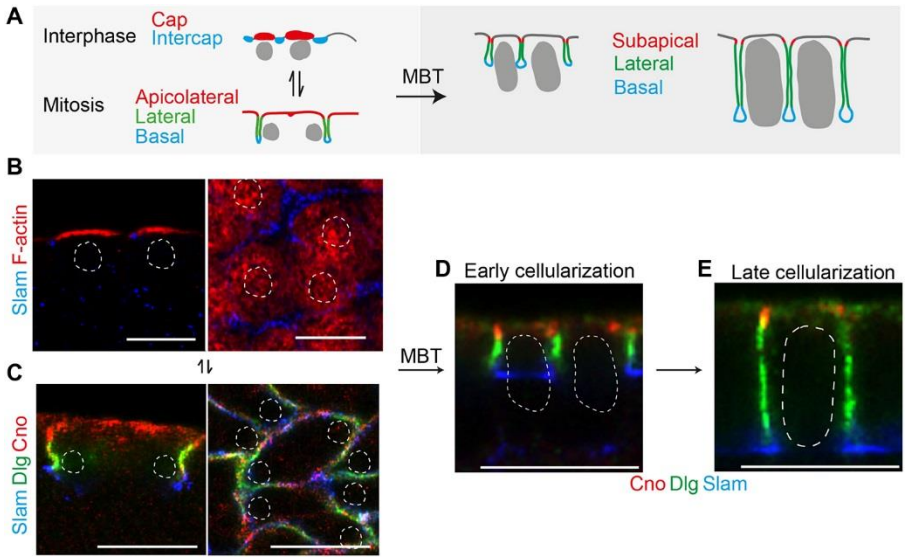

Figure 1. **Dynamics in cortical domains in the Drosophila blastoderm embryo. (A)** Scheme (sagittal view) illustrating cortical domains before and after mid blastula transition (MBT). Cap, apicolateral and subapical domains are marked in red, intercap and basal domain, in blue and lateral domain, in green. **(B–E)** Images of embryos stained for domain marker before and after MBT. **(B)** Interphase 13, stained for caps (F-actin, red) and intercap regions (Slam, blue) in sagittal and planar view. **(C)** Mitosis 12, stained for the apical-lateral (Canoe, red), lateral (Dlg, green) and basal domains (Slam, blue). Early **(D)** and late **(E)** cellularization (interphase 14), sagittal view, stained for subapical (Canoe, red), lateral (Dlg, green) and basal domains (Slam, blue). Dashed lines represent nuclei. Scale bars 10 µm.

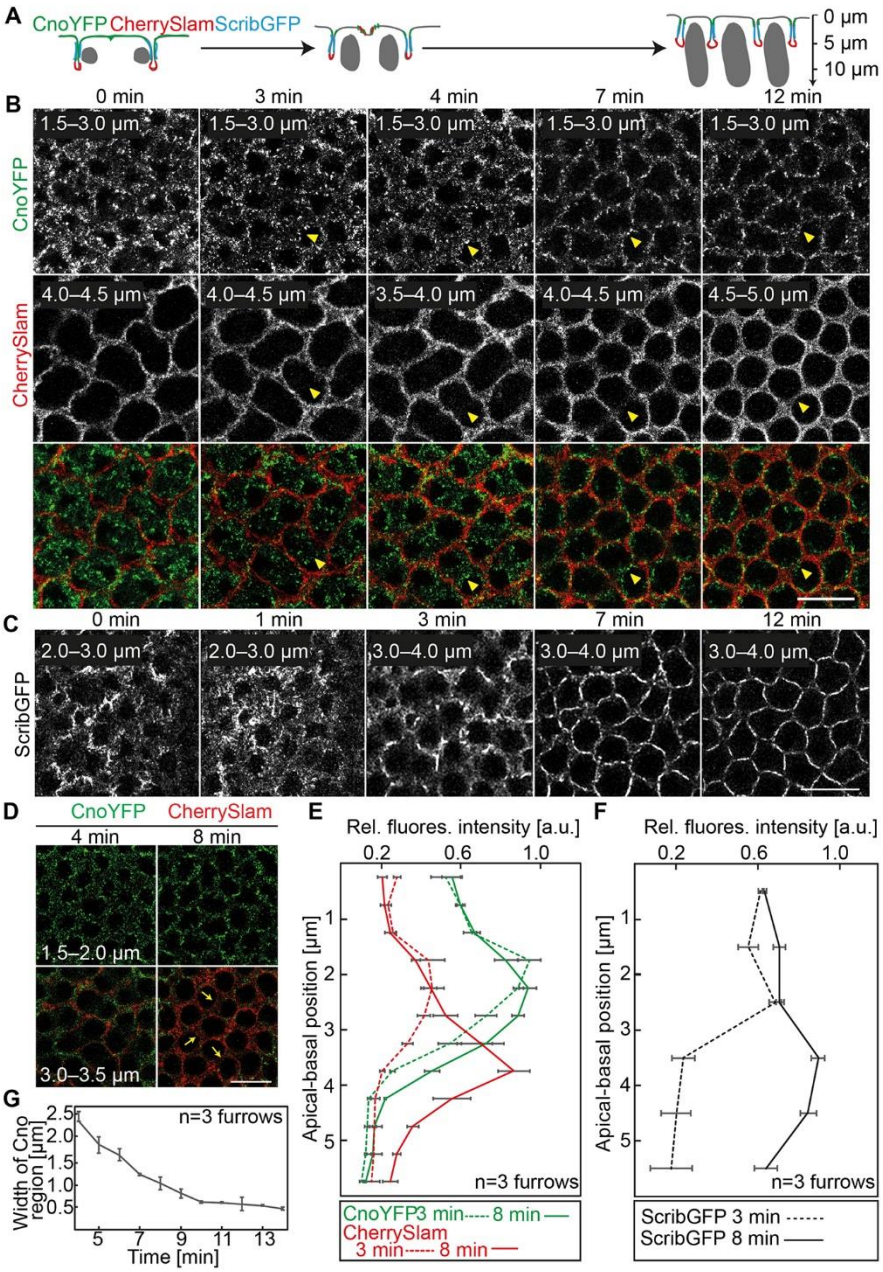

Figure 2. Dynamics of Canoe, Scribbled and Slam. (A) Scheme for furrow formation and invagination in early cellularization. CanoeYFP (green), CherrySlam (red) and ScribbledGFP (blue) mark subapical, basal and lateral domains, respectively. Axial (apical-basal) axis with approximate scale is indicated on right side. **(B–D)** Images from time lapse recordings including axial stacks of embryo expressing **(B, D)** CanoeYFP (grey/green) and CherrySlam (grey/red) or **(C)** ScribbledGFP (grey) during mitosis 13 and early interphase 14. Axial position is indicated. Yellow arrowheads point to position of "new" furrows. **(E–F)** Relative fluorescence intensity of **(E)** CanoeYFP (green), CherrySlam (red) and **(F)** ScribbledGFP at "new" furrows measured along the apical-basal axis at indicated times. **(G)** Width of CanoeYFP fluorescence signal across "new" furrows plotted against the time. Error bars represent SEM. Scale bars 10 µm.

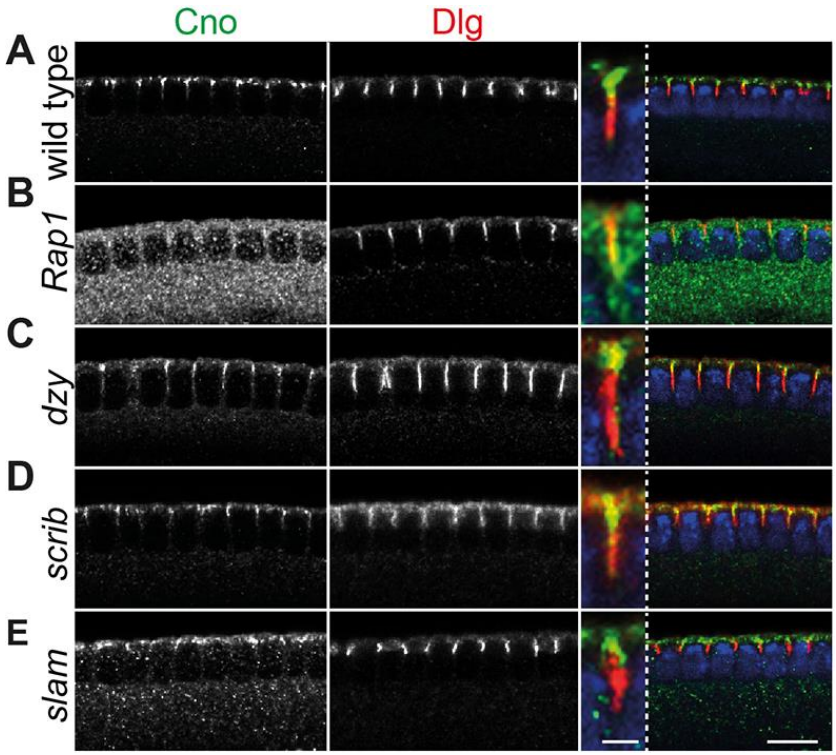

Figure 3. Genetic control of subapical Canoe. Images of fixed embryos in early cellularization stained for Canoe (grey/green), Dlg (grey/red) and DNA (blue). Merged images are shown in right panel, inserts show zoom in of one furrow. Genotypes (A) wild type, embryos from germline clones for **(B)** *Rap1*, **(C)** *dizzy,* **(D)** *scribbled*, **(E)** *slam*. Scale bars 10 µm, insets, 2 µm.

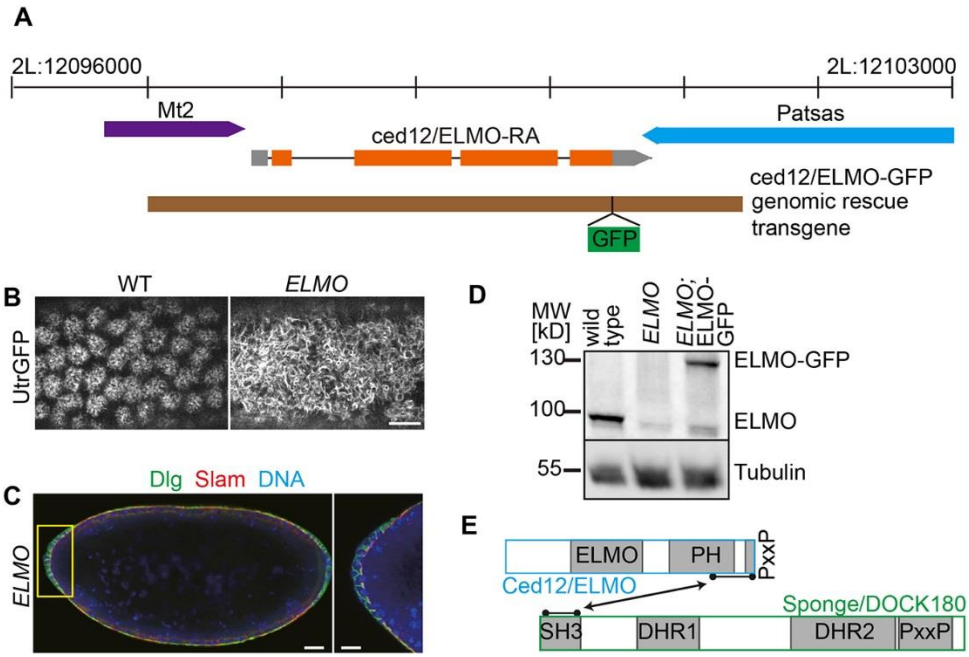

Figure 4. Blastoderm phenotype of embryos from *ELMO* germline clones. (A) ELMO locus on chromosome 2L. Genomic rescue construct ELMO-GFP is indicated by brown bar. **(B)** Images of wild type and *ELMO* embryos expressing F-actin marker UtrGFP. **(C)** Image of fixed *ELMO* embryo stained for Dlg (green), Slam (red) and DNA (blue). Cellularizing terminus marked by rectangle in yellow magnified in inset. **(D)** Embryonic extracts from wild type, *ELMO* and *ELMO* embryos with the genomic ELMO-GFP rescue transgene were analyzed by western blot with ELMO and α-Tubulin antibodies. **(E)** Domain structures of ELMO and Sponge. Interaction domains are marked by biheaded arrow. Scale bar 10 µm.

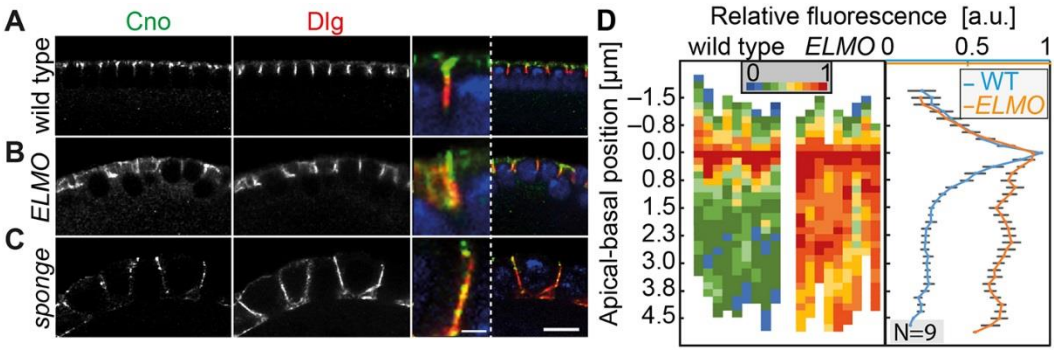

Figure 5. *ELMO* and *sponge* are required for subapical restriction of Canoe. Images of fixed wild type **(A),** *ELMO* **(B)** and *sponge* **(C)** embryos stained for Canoe (grey/green), Dlg (grey/red) and DNA (blue). Insets in higher magnification. **(D)** Heat maps and averaged values of relative fluorescence intensity along the apical basal axis for multiple furrows aligned to the peak value (nine furrow in three embryos). Error bars represent SEM. Scale bars 10 µm, inset, 2 µm.

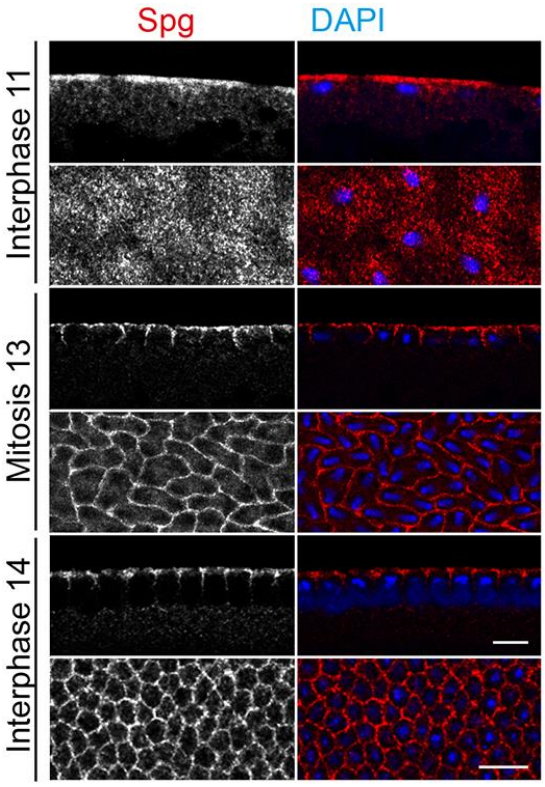

Figure 6. Subapical restriction of Sponge. Images of fixed wild type embryos at indicated stages stained for Sponge (grey/red) and DNA (blue). Sagittal and planar views. Scale bars 10 µm.

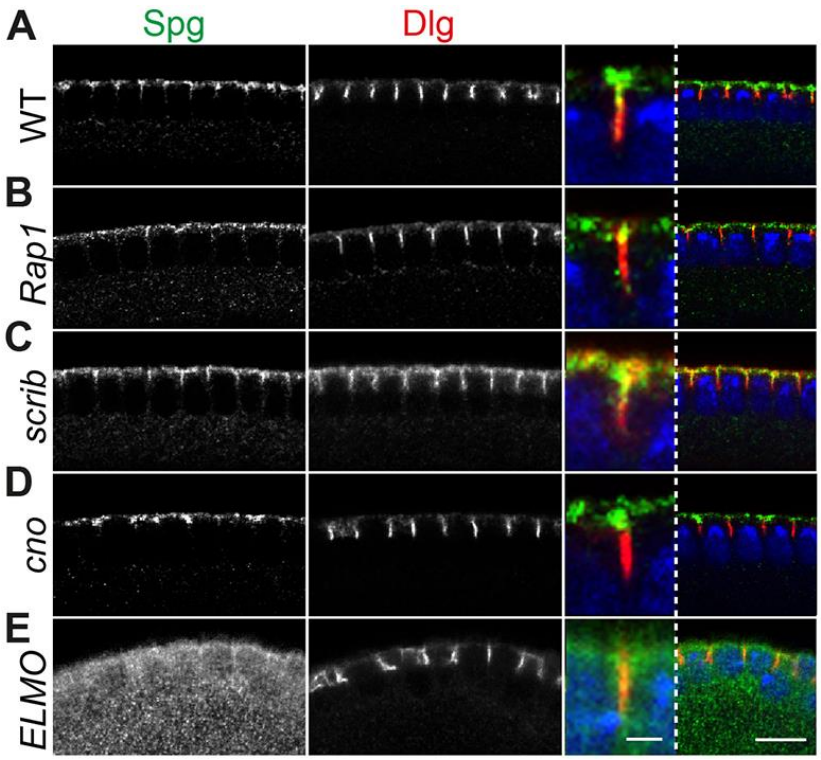

Figure 7. Genetic control of subapical Sponge. Images of fixed embryos in early cellularization stained for Sponge (grey/green), Dlg (grey/red) and DNA (blue). Merged images are shown in right panel, inserts show zoom in of one furrow. Genotypes **(A)** wild type, embryos from germline clones for **(B)** *Rap1*, **(C)** *scribbled*, **(D)** canoe, **(E)** *ELMO*. Scale bars 10 µm, insets, 2 µm.

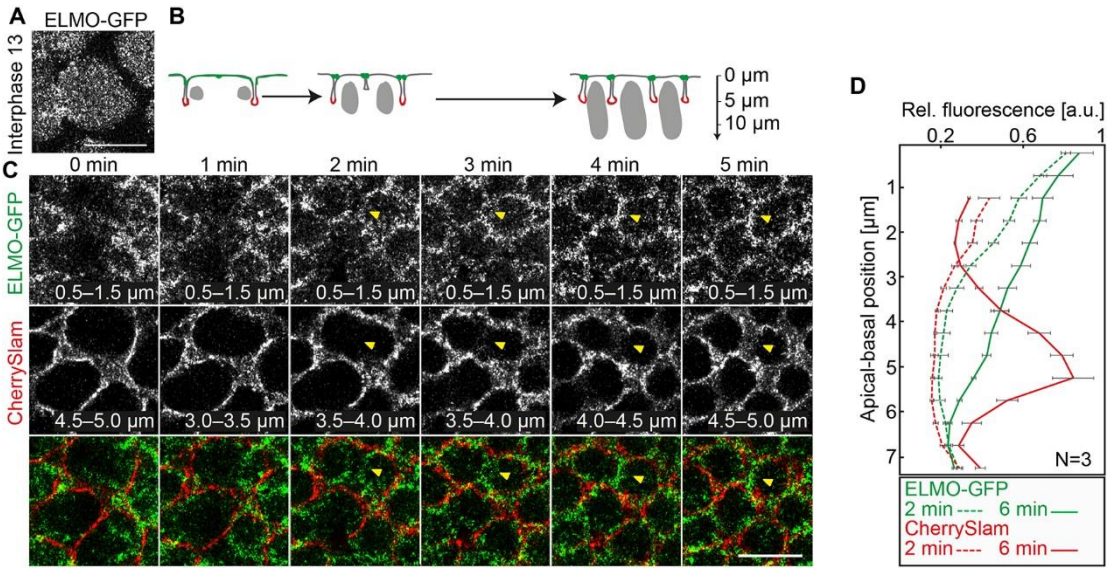

Figure 8. **Dynamics of ELMO-GFP during early cellularization. (A)** Image from a time laps recording of an embryo expressing ELMO-GFP shows ELMO-GFP localization at the cap during interphase 13. **(B)** Scheme for furrow formation and invagination in early cellularization. Subapical and basal domains are marked in green and red, respectively. Axial (apical-basal) axis with approximate scale is indicated. **(C)** Images from time lapse recordings including axial stacks of embryo expressing ELMO-GFP (grey/green) and CherrySlam (grey/red) during mitosis 13 and early interphase 14. Axial position is indicated. Yellow arrowhead point to position of “new” furrows. **(D)** Relative fluorescence intensity of ELMO-GFP (green) and CherrySlam (red) at “new” furrows measured along the apical-basal axis at indicated times (three furrows). Error bars represent SEM. Scale bar 10 µm.

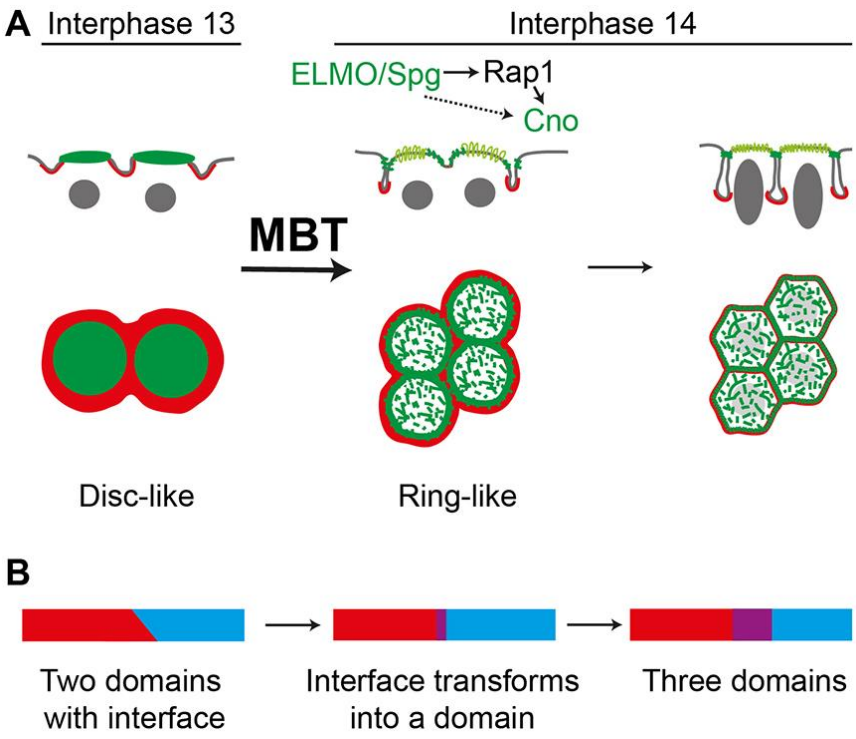

Figure 9. Model of formation of the subapical domain. **(A)** Schematic dynamics of ELMO/Sponge from disc-like to ring-like pattern during onset of interphase 14. ELMO/Sponge is a potential Rap1 activator which in turn restricts Canoe to the subapical domain. **(B)** Positional information for the emergence of the subapical domain based on transformation of the domain interface.

Supplemental data

Suppl. Figure S1

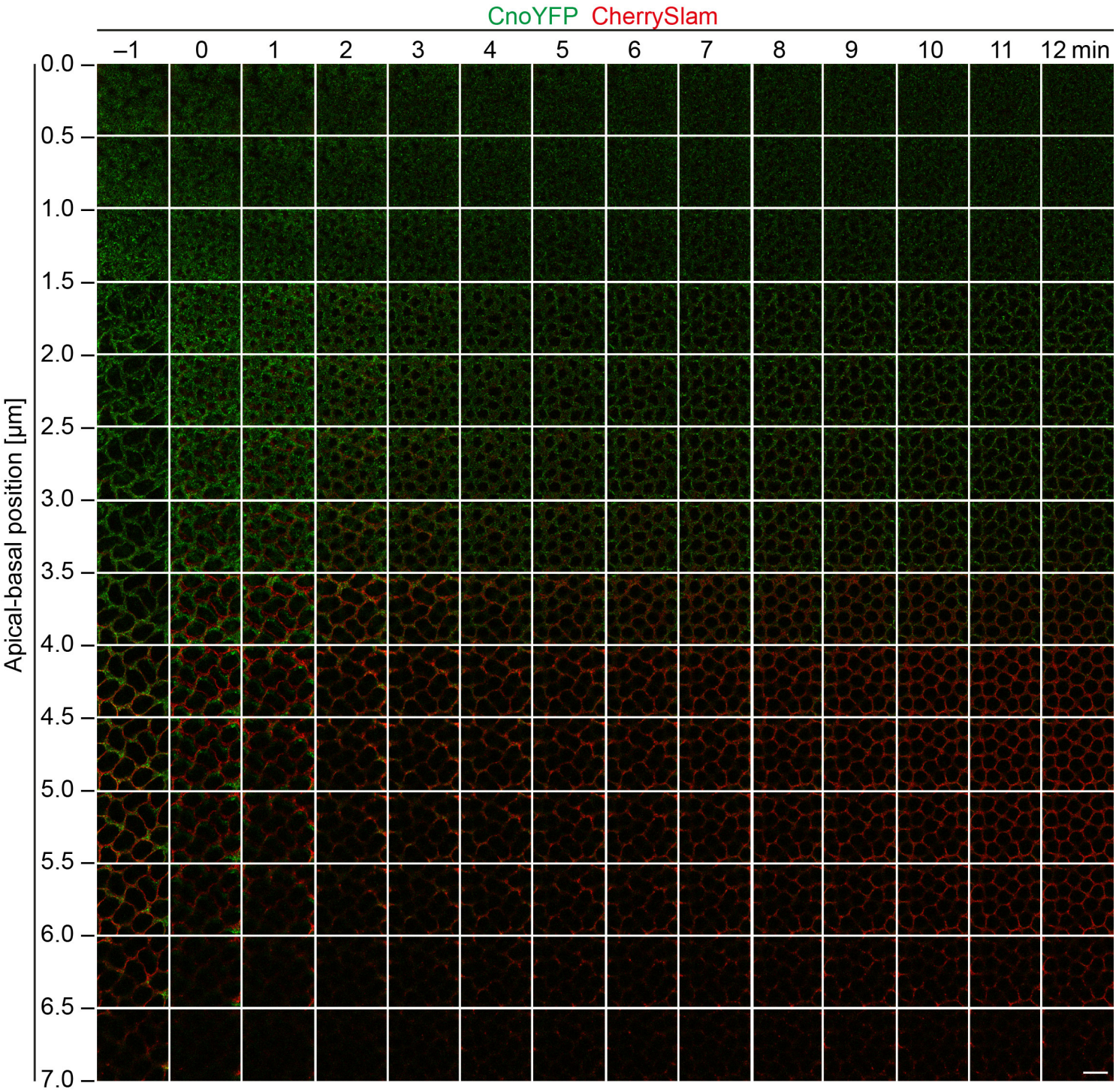

Supplemental Fig. S1. CanoeYFP and CherrySlam dynamics during mitosis 13 and interphase 14. **(A)** Images from time lapse recording of an embryo expressing CanoeYFP (green) and CherrySlam (red). Time from left to right, apical basal position from up to down. Time point t=0 was defined by the emergence of a new furrow between two corresponding daughter nuclei. The spatial difference between the two color channels at t=0 and 1 min is due to a time lag in imaging as the channels were recorded one after the other. **(B)** Scale bar 10 µm.

Suppl. Figure S2

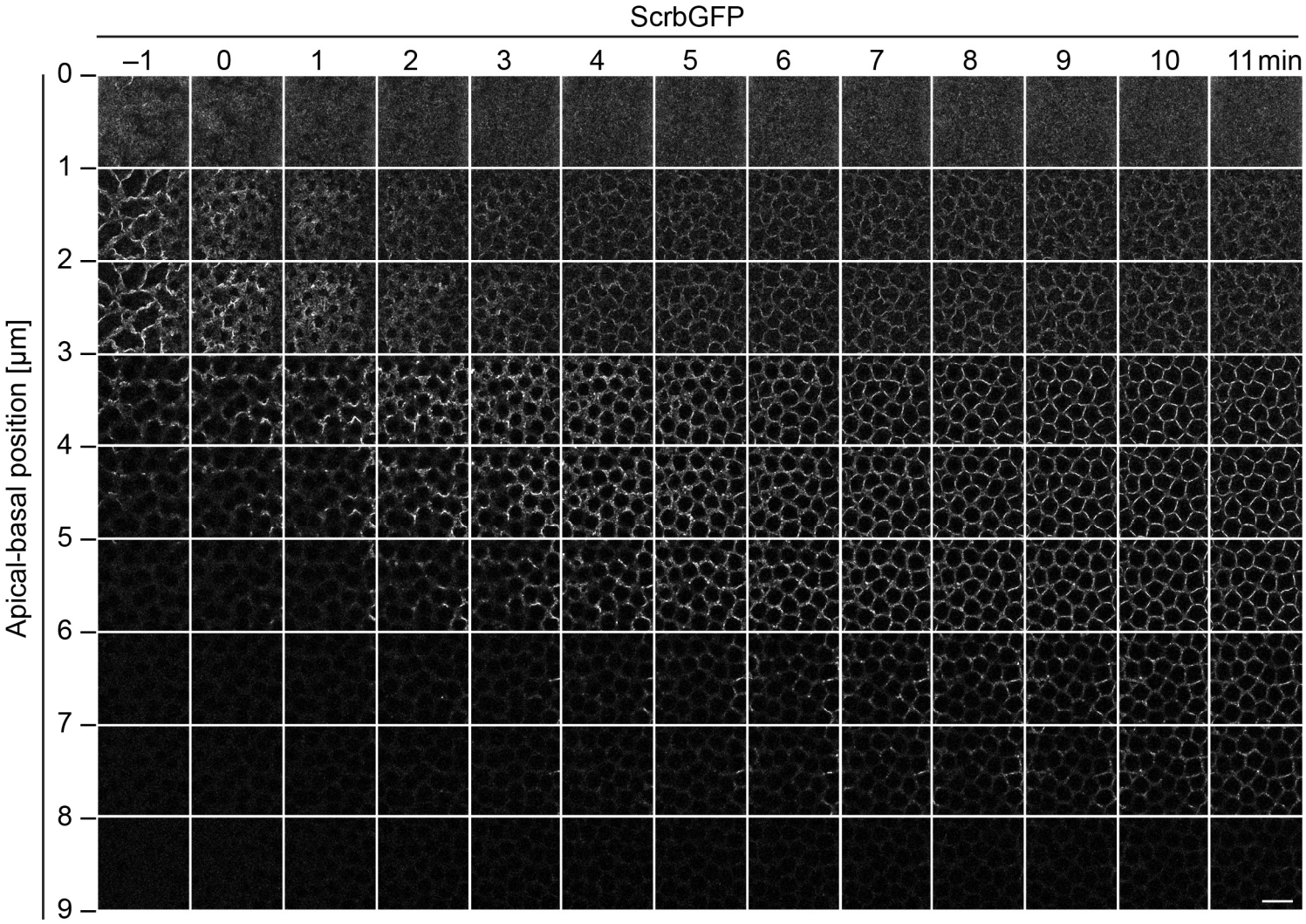

Supplemental Fig. S2. ScribbledGFP dynamics during mitosis 13 and interphase 14. Images from a time lapse recording of an embryo expressing ScribbledGFP. Time from left to right, apical basal position from up to down. Time point t=0 was defined by the emergence of a new furrow between two corresponding daughter nuclei. Scale bar 10 µm.

Suppl. Figure S3

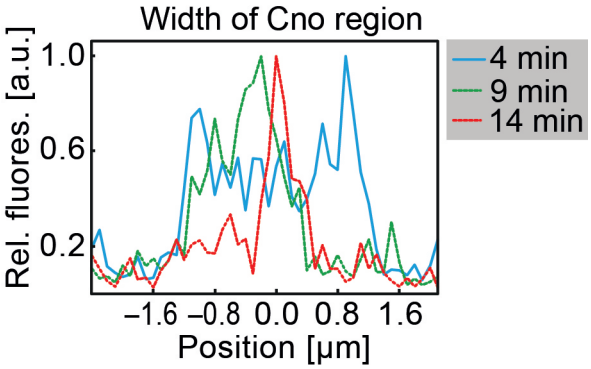

Supplemental Fig. S3. Canoe fluorescent signal narrows as the new furrow elongates. Distribution of CanoeYFP signal (relative fluorescence) across a new emerging furrow (Fig. S1) at three different time points as indicated.

Suppl. Figure S4

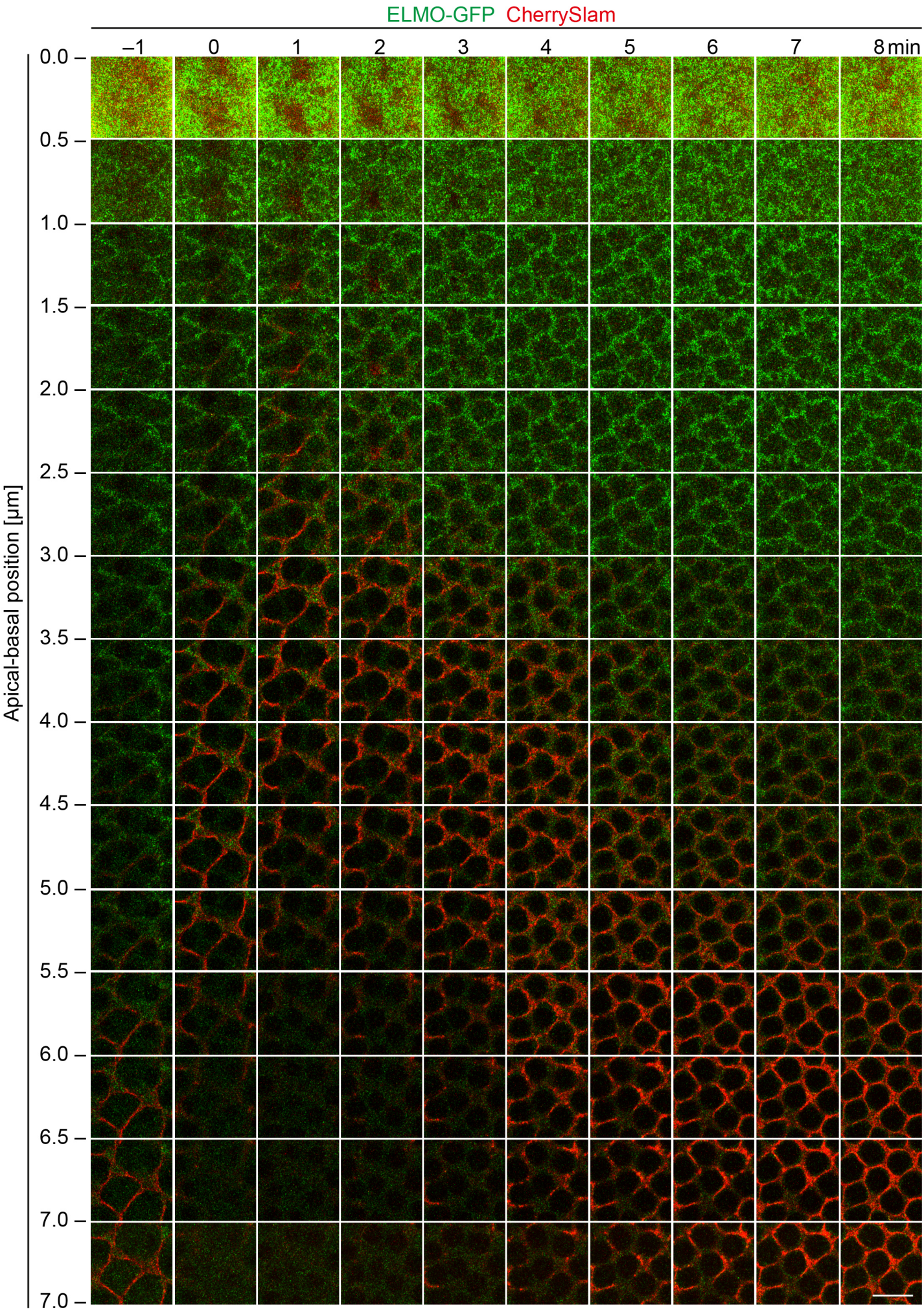

Supplemental Fig. S4. ELMO-GFP and CherrySlam dynamics during mitosis 13 and interphase 14. Images of a time lapse recording of an embryo expressing Elmo-GFP (green) and CherrySlam (red). Time from left to right, apical basal position from up to down. Time point t=0 was defined by the emergence of a new furrow between two corresponding daughter nuclei. Scale bar 10 µm.

Suppl data Fgure 5

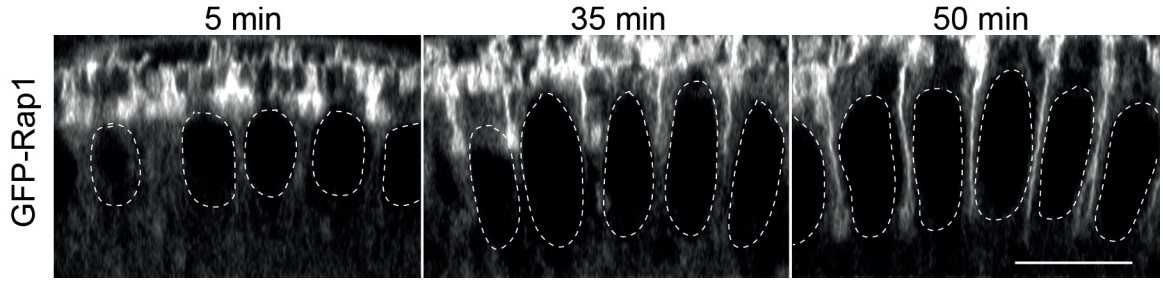

Supplemental Fig. S5. GFP-Rap1 localization during early and mid-cellularization. Images from living embryos expressing GFP-Rap1 at indicated time after onset of cellularization. Reconstructed orthogonal views from axial stacks of embryos expressing GFP-Rap1. Note that GFP-Rap1 localizes to the entire membrane without a clear enrichment at subapical, lateral or basal domain. Scale bar 10 μm.

Supplemental data

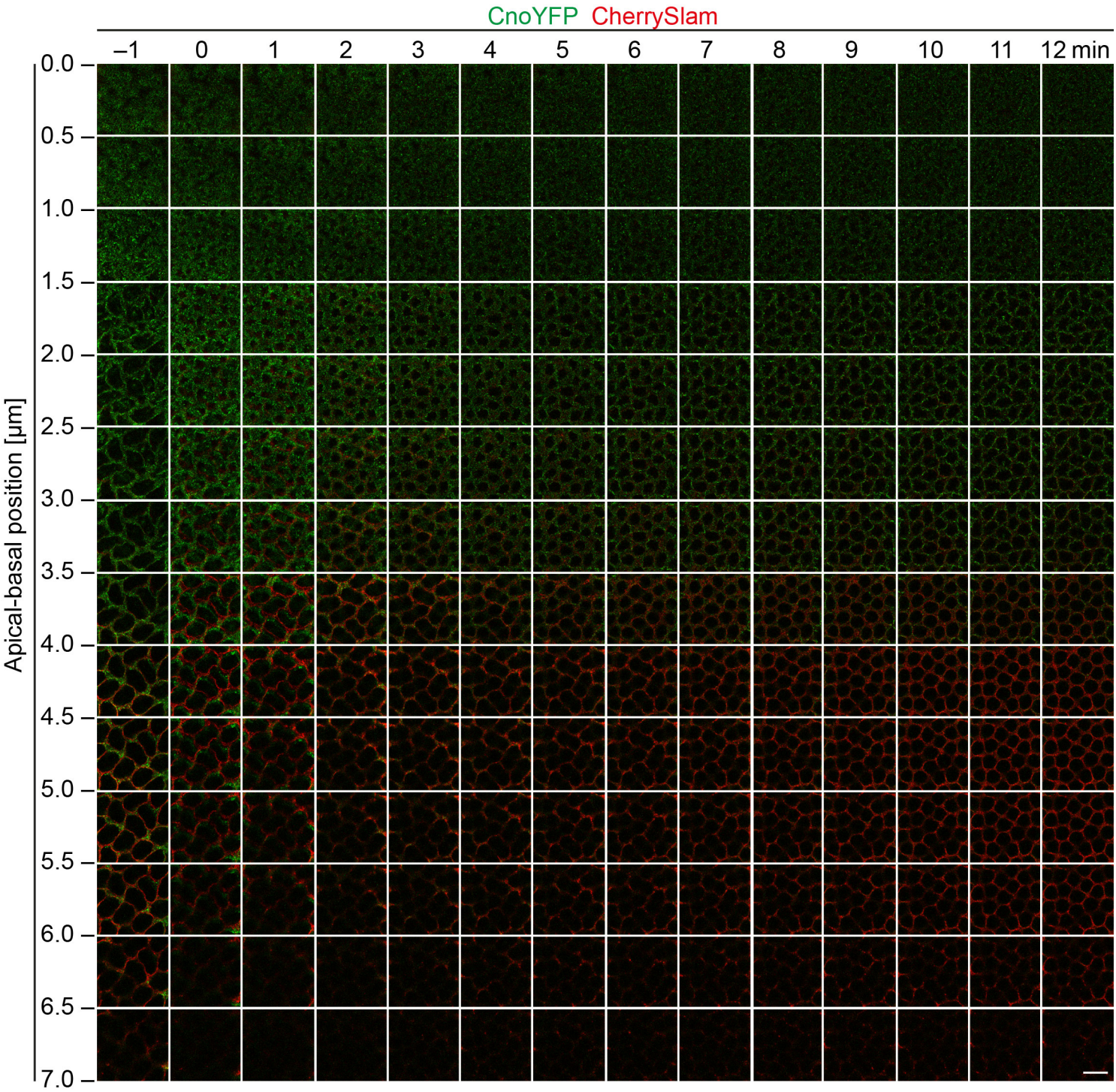

Supplemental Fig. S1. CanoeYFP and CherrySlam dynamics during mitosis 13 and interphase 14. Images from time lapse recording of an embryo expressing CanoeYFP (green) and CherrySlam (red). Time from left to right, apical basal position from up to down. Time point t=0 was defined by the emergence of a new furrow between two corresponding daughter nuclei. The spatial difference between the two color channels at t=0 and 1 min is due to a time lag in imaging as the channels were recorded one after the other. Scale bar 10 µm.

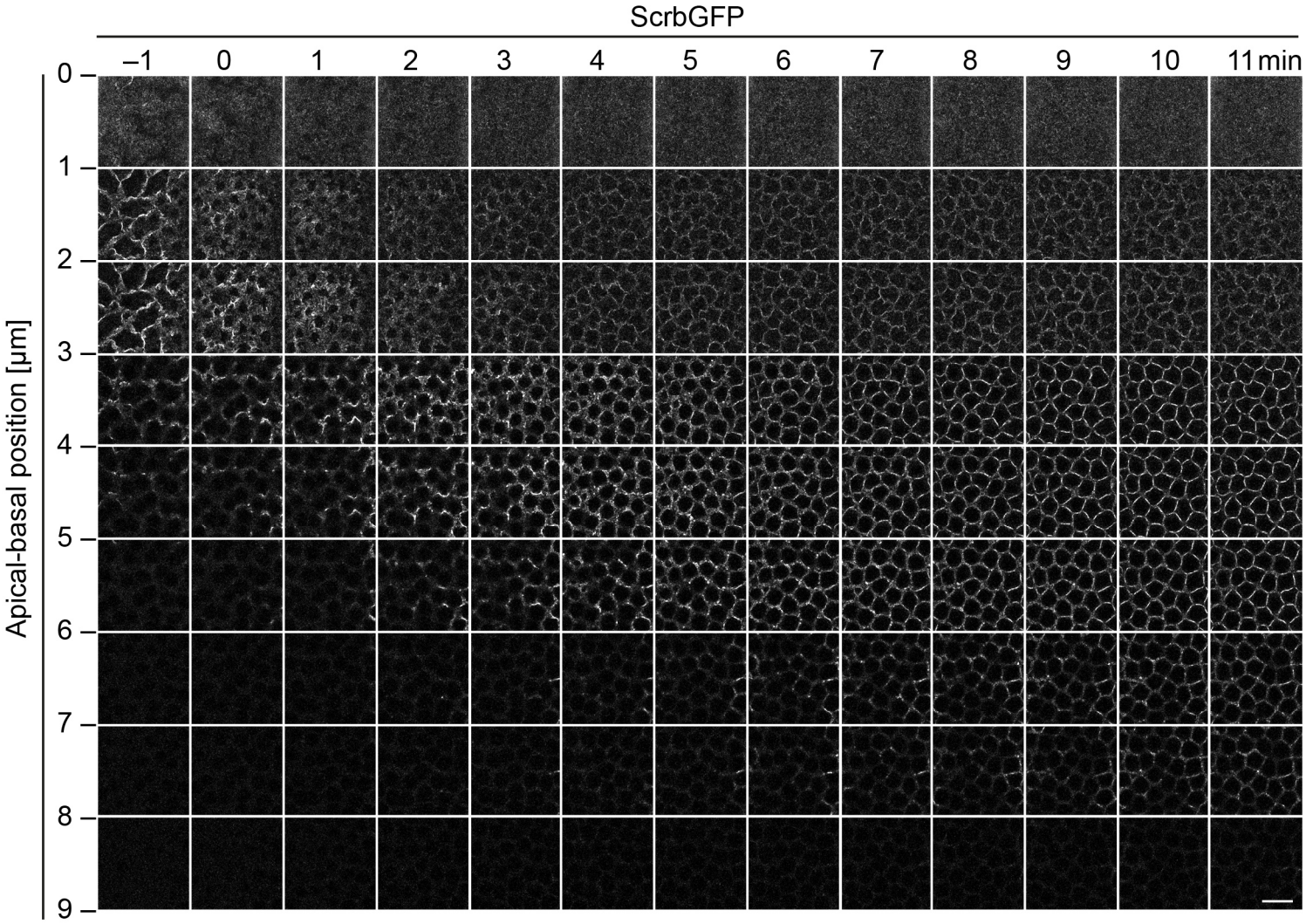

Supplemental Fig. S2. ScribbledGFP dynamics during mitosis 13 and interphase 14. Images from a time lapse recording of an embryo expressing ScribbledGFP. Time from left to right, apical basal position from up to down. Time point t=0 was defined by the emergence of a new furrow between two corresponding daughter nuclei. Scale bar 10 µm.

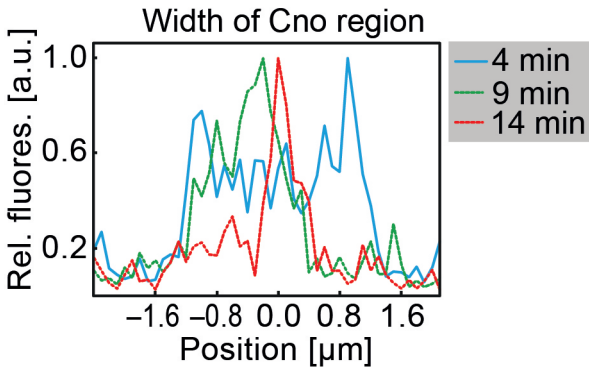

Supplemental Fig. S3. Canoe fluorescent signal narrows as the new furrow elongates. Distribution of CanoeYFP signal (relative fluorescence) across a new emerging furrow (Fig. S1) at three different time points as indicated.

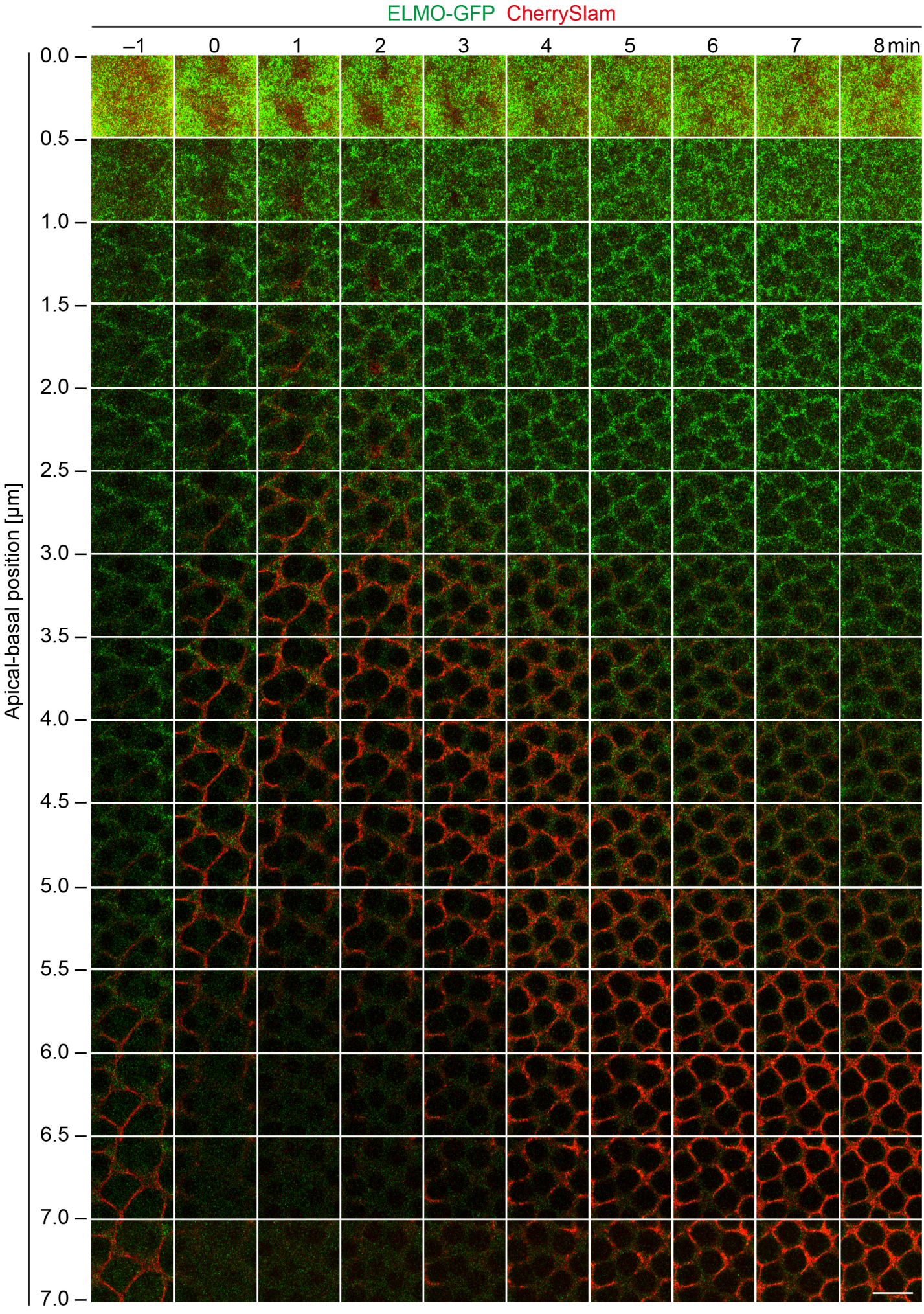

Supplemental Fig. S4. ELMO-GFP and CherrySlam dynamics during mitosis 13 and interphase 14. Images of a time lapse recording of an embryo expressing Elmo-GFP (green) and CherrySlam (red). Time from left to right, apical basal position from up to down. Time point t=0 was defined by the emergence of a new furrow between two corresponding daughter nuclei. Scale bar 10 µm.

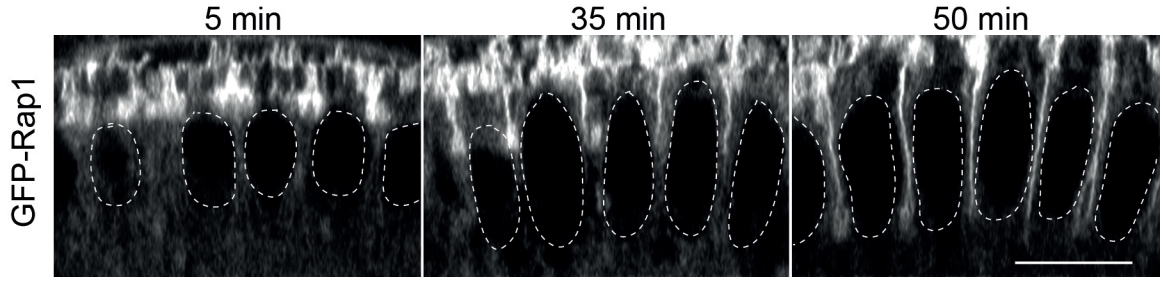

Supplemental Fig. S5. GFP-Rap1 localization during early and mid-cellularization. Images from living embryos expressing GFP-Rap1 at indicated time after onset of cellularization. Reconstructed orthogonal views from axial stacks of embryos expressing GFP-Rap1. Note that GFP-Rap1 localizes to the entire membrane without a clear enrichment at subapical, lateral or basal domain. Scale bar 10 μm.